UNIVERSITAT POLITÈCNICA DE VALÈNCIA

ETSI Aeroespacial y Diseño Industrial

**Universitat Politècnica de València**

Escuela Técnica Superior de Ingeniería Aeroespacial y Diseño Industrial

# Technical Report

*BMFA Payload Challenge 2025 - Weight class*


**Team W19**

XTRA2 UPV

May 9, 2025

# Contents

# 1. Introduction

## 1.1. The BMFA Payload Challenge and the Weight Challenge

The BMFA Payload Challenge is an aeronautics student competition held in the United Kingdom annualy. Its objective is to encourage students to design, build and fly their own unmanned aircrafts. It's organizing body, the British Model Flying Association, has been hosting design competitions at their BMFA Buckminster headquarters for over 20 years. The competition includes multiple challenges, for which different design specifications are required.

The weight challenge is a competition that is part of the BMFA Payload Challente. Its objective is the design of an aircraft capable of lifting a certain water weight, while the empty aircraft remaining as light as possible. The team's score depends on the aircrafts empty weight, and the water weight it is able to lift, but also on the evaluation of the technical quality of the project's design reports, drawings and presentation.

## 1.2. UPV and Xtra2UPV

The Polytechnic University of Valencia (UPV) is a Spanish university located in Valencia. It has a focus on engineering and the physical sciences, being a top research university in the field of thermofluid dynamics.

XTRA2 UPV is a student team whose objective is the development of Unmanned Aerial Vehicle (UAV) design. It was founded in 2018 to participate in the Air Cargo Challenge. Since then, it has participated in numerous competitions, achieving a fourth place in the 2022 Air Cargo Challenge, and a fifth place in the 2024 Air Cargo Challenge. The team has also founded its own competition, the XtraChallenge, in order to fill the lack of aerospace student competitions in Spain.

XTRA2 UPV aims to provide students with hands-on knowledge of aircraft development, complimenting their education in more theory-dense subjects that cover this same topic.

## 1.3. Purpose

This report summarizes the development of the XTRA26, the aircraft that XTRA2 UPV will present to the BMFA Payload Challenge (Weight Challenge), in Buckminster. It explains the steps that have had to take place in order to arrive at the finalized design, as well as the manufacturing of the aircraft.

# 2. Project Management

## 2.1. Team Structure

As per competition regulations, a selection of 7 XTRA2 members compose the team whose responsibility is the development and design of the aircraft. Other XTRA2 members are assigned to the social media and marketing departments of the team, as well as teams building their own aircraft for the XtraChallenge national competition.

In 2.1 the organization of the team is presented. The team consists of Bachelors' students of the UPV, as well as a professor in charge, Dr Pedro Manuel Quintero Igeño.

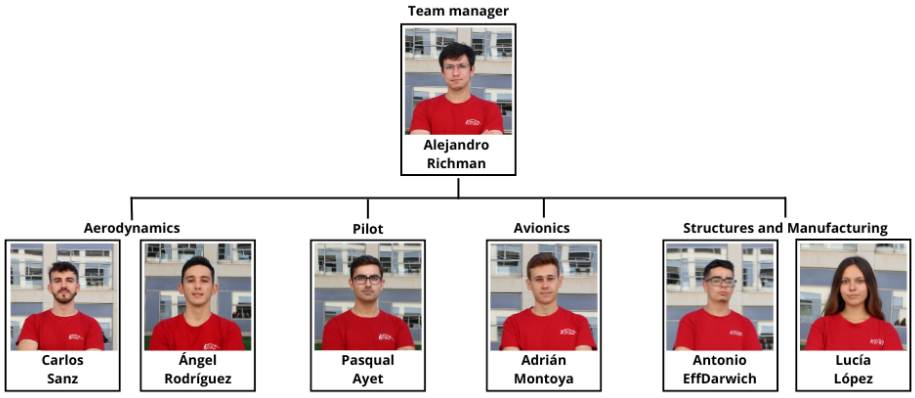


**Figure 2.1:** Team members

## 2.2. Planning and schedule

In order to meet the goal of the competition, correct planning of time and resources is crucial. To manage this, a schedule was created where deadlines were managed in September. Though it later changed, the development goals were met before the turning in of the report.

The following schedule, in 2.2, represents the work schedule followed throughout the year in the development of the aircraft.

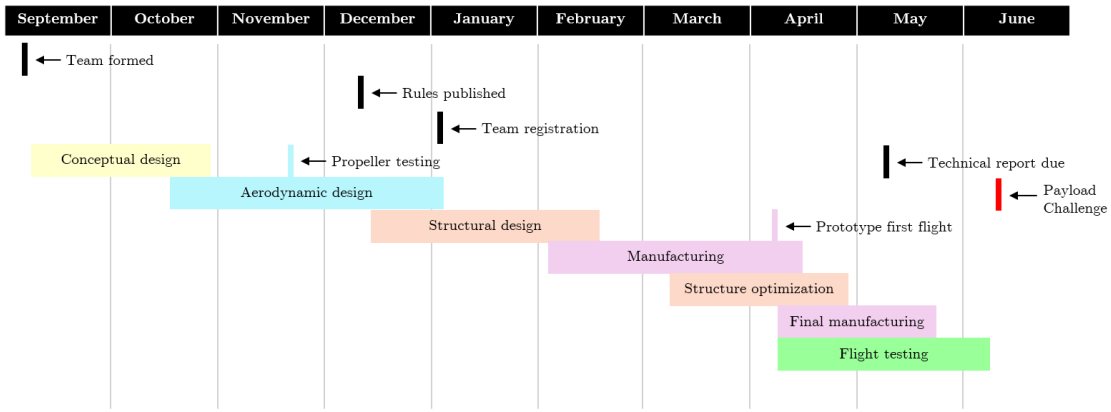


**Figure 2.2:** Gantt organization chart

## 2.3. Sponsors and Collaborators

**Generación Espontánea:** It is an educational program of the UPV. Through assesment and funding, it seeks to promote student initiative, by helping and providing resources for a large array of student groups interested in participating in competitions and hackathons. During the 2024/2025 academic period, it has provided XTRA2UPV with 11,365€ to support XTRA2's proper functioning, with which materials and tools are acquired.

**Escuela Técnica Superior de Ingeniería Aeroespacial y Diseño Industrial:** It is a department of the UPV that specialises in mechatronic and aerospace engineering. It is in charge of imparting, amongst others, the B.Eng. in Aerospace Engineering. It has provided 2100€ to cover the cost of shipping and flights for the team members to the competition.

**Sika:** A multinational chemicals manufacturer, it provides the team with commonly used materials in the manufacturing process, such as epoxi resin, structural adhesive, demolding wax, and PUR tooling board. It has provided upwards of 2500€ in materials for the whole team over two years.

**Siemens:** A multinational technology conglomerate, it provides the team with much needed analysis softwares such as StarCCM+, or NX. It provides the team with licences to its software, valued at 500000€

**Club d'aeromodelisme l'Abella:** An RC flying club in the south of Valencia, it provides the team with access to its flying grounds for flight testing and hands-on advice. It is also the host of the XtraChallenge, the competition that XTRA2UPV organizes.

# 3. Conceptual Design

## 3.1. Mission Analysis

The team was formed in August 2024. Anticipating minimal changes in the competition rules based on previous editions, the design team conducted a thorough analysis of the mission requirements. The team established a set of design targets for the XTRA-26 aircraft, ahead of the official release of the 2025 Flight Challenge 5 – Weight ruleset. The primary performance metric of the competition is the ratio of payload (liquid plus receptacle) to empty aircraft weight, with the aircraft being required to take off, complete a defined flight pattern, and land within a strict timeframe using a standardized electric propulsion system.

The key constraints and performance goals derived from the rules are:

- Fixed-wing aircraft only, without rotating lifting surfaces.
- Specified propulsion system: 4-Max PO-3541-1070 motor, 4M-ESC50AV2 ESC, and one 3S 2200mAh LiPo battery per round, provided by the organizers.
- Removable payload containers for liquid, up to 4.0 kg total scoring mass.
- Robust, easily inspectable integration of isolator (XT60-Wall), safely mounted behind the propeller arc.

The competition scoring system prioritizes not only the ability to carry high payloads but also emphasizes a lightweight structure and stable flight characteristics. This duality —maximizing structural efficiency while preserving aerodynamic performance— defined the entire design strategy.

## 3.2. Conceptual Sketch

### 3.2.1. Initial Concept

The project began with a clean-sheet design based on a high-aspect-ratio monoplane featuring elliptical wingtips, a streamlined fuselage, and a V-tail empennage. The water payload was to be loaded internally in longitudinally arranged removable containers, aligned near the aircraft's center of gravity. This design aimed to minimize aerodynamic

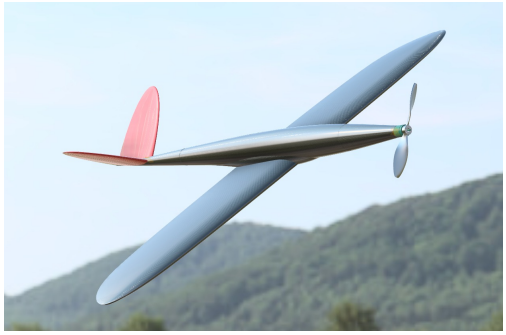

**Figure 3.1:** Initial concept design

drag, optimize lift distribution, and
exploit glide efficiency—principles derived from sailplane and high-efficiency UAV design.

The aircraft featured a tractor-mounted electric motor, a fixed landing gear, and a high-mounted main wing. A pair of flaperons—control surfaces combining the functionality of flaps and ailerons—were included from the start to reduce weight and simplify the actuation system, eliminating the need for redundant surfaces and servos.

However, early assessments revealed limitations in payload accessibility, mass distribution, and fuselage structural complexity. The team recognized that internal payload storage, while aerodynamically clean, penalized the design in terms of modularity and reconfigurability. These drawbacks motivated a major conceptual shift.

### 3.2.2. Evolved Configuration

Following several iterative design sessions and subsystem trade-offs, the concept evolved into a dual-wing configuration: a primary lifting wing located in a high-wing position, and a secondary lower wing dedicated to payload carriage. This setup provides distinct advantages for the mission requirements:

- Decoupling of structural and payload functions: the upper wing is optimized purely for aerodynamic efficiency, while the lower wing is designed to securely hold modular payload containers filled with liquid.
- Improved modularity: the lower wing can be detached or replaced independently of the main structure, allowing easier scrutineering and maintenance.
- Enhanced lateral stability: placing the payload mass beneath the main wing creates a pendulum effect, increasing roll stability and improving control during take-off and landing.
- Reduced fuselage complexity: eliminating the need for an enclosed payload bay allowed for a slimmer, lighter central fuselage structure.

This new configuration retains the original V-tail, chosen for its ability to reduce wetted surface area and component count. By combining pitch and yaw control into a single control surface pair, the V-tail reduces total mass and drag while offering sufficient authority for all flight regimes. Its 40° dihedral was fine-tuned through simulation to maintain longitudinal and directional stability.

Additionally, the landing gear is arranged in a fixed taildragger configuration, with sufficient clearance between the lower and upper wings to allow safe operation on grass fields and access to the payload receptacles. The isolator (XT60-Wall type) is mounted in a rear-facing, visible position behind the propeller arc, meeting all contest safety and accessibility requirements.

# 4. Electronic Systems and Propulsion

## 4.1. Prior Considerations

Due to regulations, several components are standard across all teams.

The designated motor model is the unmodified 4-Max PO-3541-1070. The aircraft is propelled by a single motor operating in direct drive and a single propeller. Propeller selection remains unrestricted. The power system is completed by a 4M-ESC50AV2 speed controller. These components are powered by a single 3 cell Lithium Polymer battery PPL-60C3S-2200 of 2200 mAh nominal capacity, as specified by the regulations. As a required safety measure, the aircraft includes an XT60-Wall isolator unit to disconnect the battery from the speed controller when the isolator plug is removed.

## 4.2. Propeller Selection

To define the prototype's propeller, several models were evaluated through both computational simulations and experimental testing [1]. The final selection was based on multiple criteria, including thrust performance and engine compatibility, resulting in the choice of a 13x7 propeller.

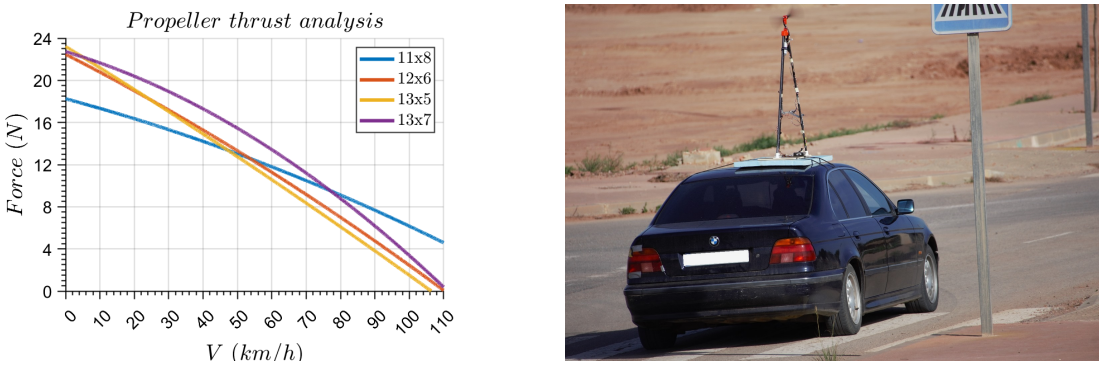


**(a)** Thrust generated by the propellers

**(b)** Experimental tests

**Figure 4.1:** Propeller results and testing

For the calculation of power loading, the power has been estimated by measuring both the voltage and amperage of the motor, using a 40 Amp power supply.

| Configurations | OEW aircraft | 2kg Cargo | 4kg Cargo |
|---|---|---|---|
| **Power Loading (N/W)** | 0.019 | 0.055 | 0.089 |

**Table 4.1:** Power loading

## 4.3. Freely Selectable Electronic Components

### 4.3.1. Servomotors and Receiver (Rx)

The selection of servomotors focuses on lightweight components, which must be seamlessly integrated within the aircraft's structure. In addition, this selection is based on rigorous calculations to determine the maximum forces the servomotors must withstand.

KST X08H Plus servomotors were chosen for their reliability, compactness and robust performance. The use of metallic gear servomotors enhances durability and functionality. Furthermore, their light design, weighing at only 9g, perfectly suits the application.

These servos provide a working torque of 5.3 kg·cm at 8.4 V, reaching the needed value, which has been computed by means of the empirical Equation (1). In this calculation, $c_f$ is the chord of the moving surface in cm, $b_f$ its length in cm, $V$ stands for the airspeed in mph, $\delta_f$ represents the deflection of the given surface, and $\theta_f$ is the operational range of the servo from the neutral point.

$$T_{\text{servo}} = 6.12 \cdot 10^{-7} \cdot \frac{V^2 \cdot c_f^2 \cdot b_f \cdot \sin(\delta_f) \cdot \tan(\delta_f)}{\tan(\theta_{\text{servo}})} \quad [\text{kg} \cdot \text{cm}] \tag{1}$$

The receiver of choice was a FlySky iA6B due to its reliability and availability within the team's resources. It is compatible with the radio we use, a TX16S.

## 4.4. Circuit

Figure 4.2 shows the layout of all electronic components used in the aircraft.

Two servos actuate the tail's moving surfaces and two are in charge of the flaperons. The motor, open to the airflow, is securely screwed to the nose of the aircraft. The ESC, battery and receiver are located on the nose of the airplane too.

In compliance with regulations, the circuit includes an isolator unit that enables rapid disconnection between the battery and the rest of the system.

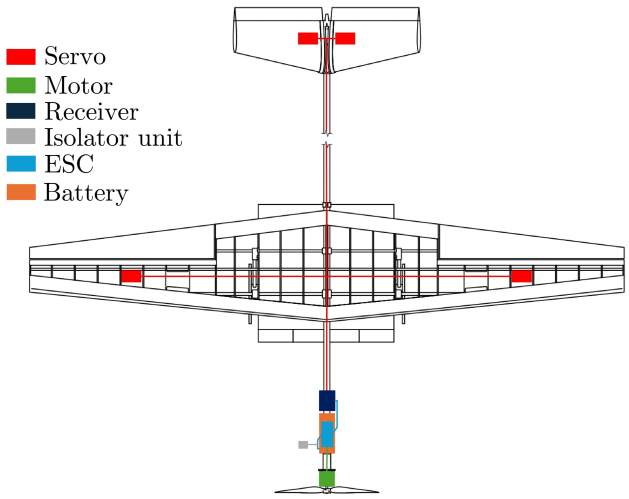


**Figure 4.2:** Electronic circuit diagram

# 5. Aerodynamic Design

## 5.1. Main Wing Design

During the design phase, several aircraft configurations were analyzed, ultimately leading to the final design of the aircraft, using [2] as reference. Table 5.1 presents the key dimensions of the main wing.

| $S_w(m^2)$ | $b_w(m)$ | $c_w(cm)$ | $\lambda_w$ | $\Lambda_{c/4,w}$ (°) | $\theta_{t,w}$ (°) | $\Gamma_w$ (°) | $AR_w$ |
|---|---|---|---|---|---|---|---|
| 0.336 | 1.6 | 22 | 0.4 | 3.93 | -0.5 | 0 | 7.63 |

**Table 5.1:** Main wing characteristics

One of the most distinctive design choices on the main wing is the use of flaperons. This configuration allows the ailerons to also function as simple flaps during takeoff and landing. Although not the most aerodynamically efficient flap system, it offers the advantage of reduced weight. In this aircraft, the ailerons are wider than those on a typical design, as the flaperons play a critical role during takeoff. This modification impacts certain flight characteristics, which will be discussed later.

| $S_f(m^2)$ | $b_{i,w}(m)$ | $b_{t,w}(m)$ | $\%c_{i,w}$ | $\%c_{t,w}$ |
|---|---|---|---|---|
| 0.031 | 0.375 | 0.8 | 40 | 25 |

**Table 5.2:** Flaperons dimensions (per side)

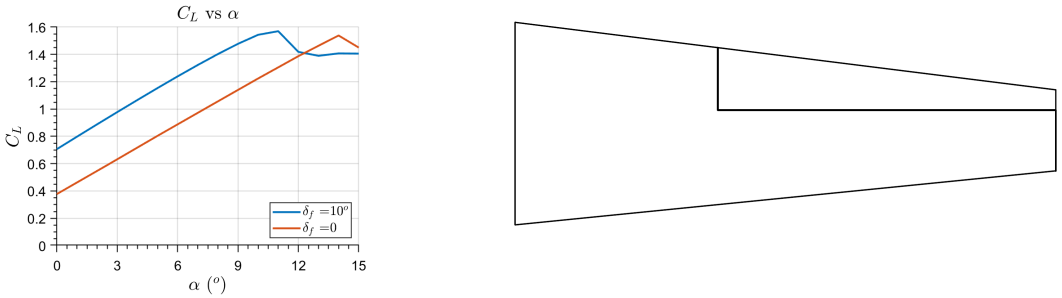


**(a)** Lift coefficient with and without flaperons **(b)** Top view

**Figure 5.1:** Main wing with flaperons

## 5.2. Cargo Bay

For the cargo bay, a wing-mounted design has been selected. The primary objective of this decision is to optimize flight dynamics while considering loading and

manufacturing constraints. The main characteristics are presented in Table 5.3.

| $S_w(m^2)$ | $b_{w2}(m)$ | $c_{w2}(cm)$ | $\lambda_{w2}$ | $\Lambda_{c/4,w2}$ (°) | $\theta_{t,w2}$ (°) | $\Gamma_{w2}$ (°) | $AR_{w2}$ |
|---|---|---|---|---|---|---|---|
| 0.13 | 36.5 | 36.5 | 1 | 0 | 0 | 0 | 1 |

**Table 5.3:** Second wing dimensions

The configuration of both wings is shown in Figure 5.2. This positioning was chosen based on the aircraft's center of gravity when the tank is full, ensuring overall stability. Although this is not a conventional solution, shifting the second wing forward has proven beneficial for the aircraft's stability characteristics. The main drawback of this configuration is the potential for flow separation on the main wing caused by the stall of the second wing. However, since the aircraft is not expected to operate at high angles of attack, the likelihood of this phenomenon occurring is significantly reduced.

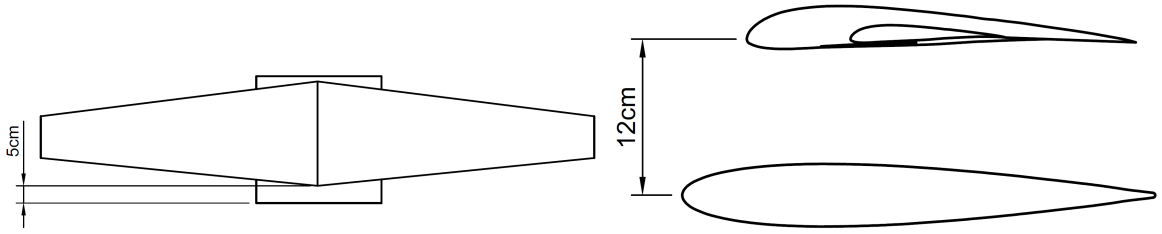


**(a)** Top view **(b)** Lateral view

**Figure 5.2:** Distance between both wings

## 5.3. Empennage Design

The selected tail design is a V-tail configuration. This choice allows for a reduction in the number of required actuators, contributing to overall weight savings. The main characteristics and dimensions of this design are presented in Table 5.4.

| $S_t(m^2)$ | $b_t(m)$ | $b_{t,proj}(m)$ | $c_t(cm)$ | $\lambda_t$ | $\Lambda_{c/4,t}$ (°) | $\theta_{t,t}$ (°) | $\Gamma_w$ (°) | $AR_t$ |
|---|---|---|---|---|---|---|---|---|
| 0.09 | 0.62 | 0.47 | 15 | 0.69 | 7.58 | 0 | 40 | 4.2 |

**Table 5.4:** Tail dimensions

The control surfaces are dimensioned to function as both elevators and rudders, depending on how they are actuated. When the same deflection angle is applied to both surfaces, they operate as pure elevators. If different angles are applied, the actuation produces a combination of longitudinal and lateral-directional effects. The dimensions of the control surfaces are presented in Table 5.5.

| $S_{control}(m^2)$ | $\%c_{r,t}$ | $\%c_{t,t}$ |
|---|---|---|
| 0.011 | 20 | 29 |

**Table 5.5:** Empennage control surfaces dimensions (per side)

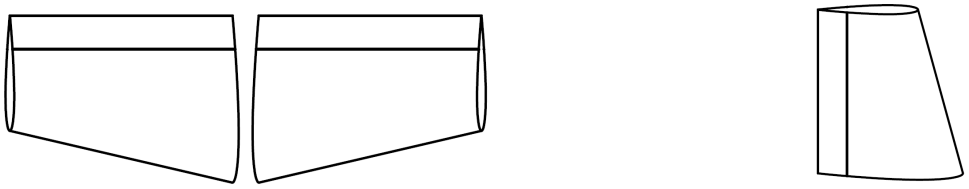

**(a)** Top view **(b)** Lateral view

**Figure 5.3:** Empennage

## 5.4. Airfoil Selection

Moving on to airfoil selection, several options were evaluated using the team's CFD software, STAR-CCM+, as well as XFLR5, to ensure optimal aerodynamic performance. Initially, a range of airfoils were tested through both 2D and 3D simulations to assess their capabilities. Based on these results, the aerodynamics team proceeded to refine the selected profiles to improve pressure distribution along the chord. The final airfoils selected are listed in Table 5.6.

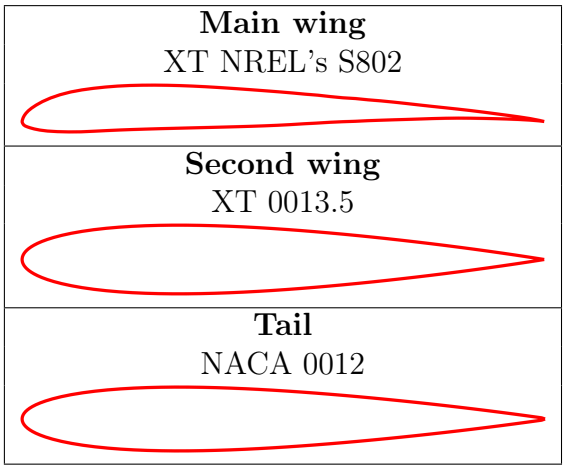


**Table 5.6:** Airfoil selection

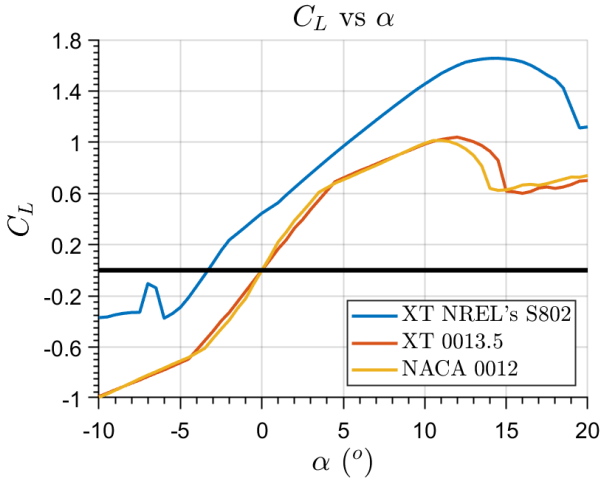


**Figure 5.4:** 2D Airfoils Characteristics

| | Thickness | Position | Camber | Position |
|---|---|---|---|---|
| **XT NREL's S802** | 10.5 % | 20.6 % | 3.5 % | 30.1 % |

**Table 5.7:** Main Wing Profile Geometric Characteristics

## 5.5. Complete aircraft

To summarize the aerodynamic design, this section concludes with the presentation of polar plots, the equations defining the linear aerodynamic range, and the lift distribution across the wingspan for both single and dual-wing configurations (Figure 5.5). To further improve the design, STAR-CCM+ was used to optimize wing–tail interactions, enhance lift distribution, and reduce the drag caused by the integration of the landing gear. [3]

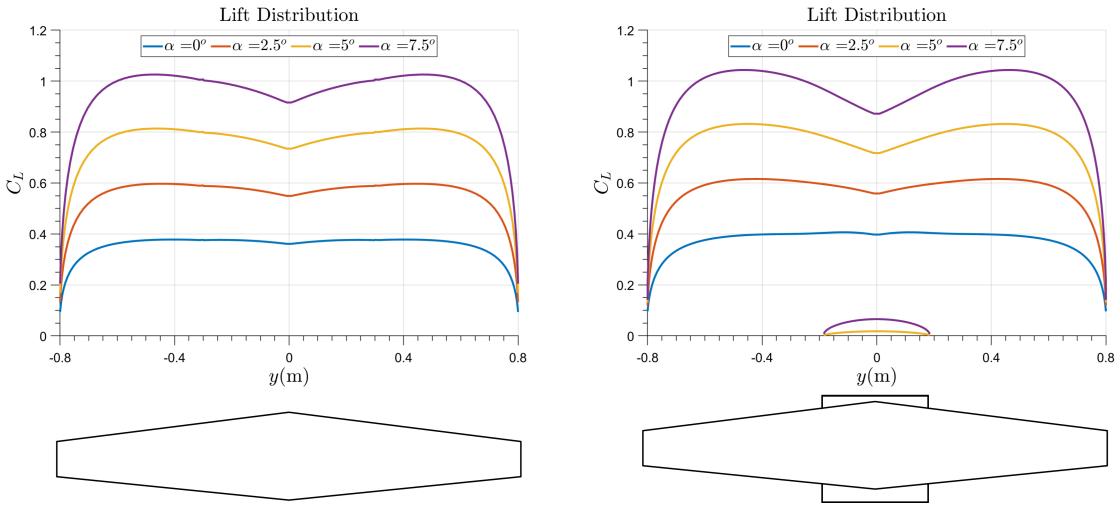


**Figure 5.5:** Lift distribution on the wings on different configurations

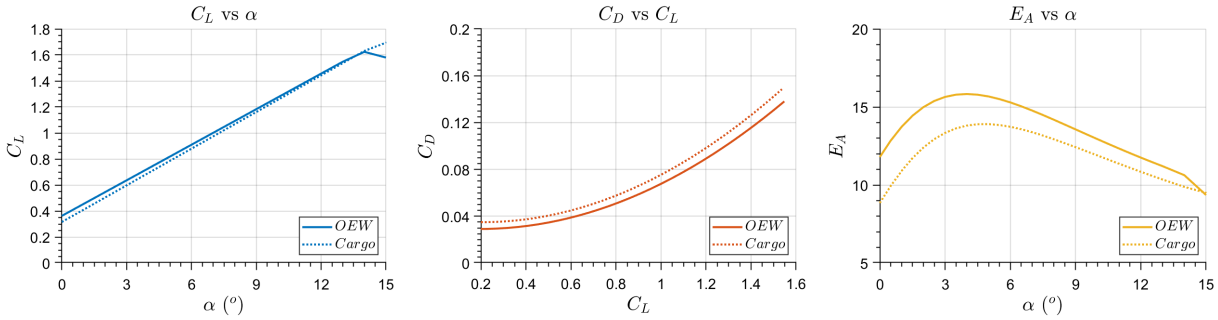


**(a)** Lift Coefficient **(b)** Drag Coefficient **(c)** Aerodynamic Efficiency

**Figure 5.6:** Aerodynamic performance of both configurations

$$\text{Linearised lift coefficient (OEW):} \quad C_L = 0.363 + 5.22 \cdot \alpha$$

$$\text{Linearised drag coefficient (OEW):} \quad C_D = 0.0291 + 0.0596 \cdot (C_L - 0.1959)$$

$$\text{Linearised lift coefficient (Cargo):} \quad C_L = 0,316 + 5.38 \cdot \alpha$$

$$\text{Linearised drag coefficient (Cargo):} \quad C_D = 0.0349 + 0.0639 \cdot (C_L - 0.2042)$$

# 6. Flight Mechanics

## 6.1. Weight Distribution

The weight distribution of the various components of the aircraft is provided in Table 6.1.

| Part | xCog (cm) | yCog (cm) | zCog (cm) | Mass (kg) |
|---|---|---|---|---|
| Right half wing | 16 | 32 | 0 | 0.265 |
| Left half wing | 16 | -32 | 0 | 0.265 |
| Right half tail | 92 | 10 | 11 | 0.087 |
| Left half tail | 92 | -10 | 11 | 0.087 |
| Engine | -47 | 0 | -1.5 | 0.127 |
| ESC | -38 | 0 | 0 | 0.041 |
| Main battery | -34.5 | 0 | -0.034 | 0.17 |
| Receiver | -10 | 0 | 0 | 0.008 |
| **Empty Aircraft** | 8.6 | 0 | 0.9 | 1.095 |
| Cargo Bay Structure | 11.5 | 0 | -12 | 0.4 |
| Right Tank | 12.5 | 13.6 | -12 | 1 |
| Central Tank | 12.5 | 0 | -12 | 1.6 |
| Left Tank | 12.5 | -13.6 | -12 | 1 |
| **Full Aircraft** | 11.6 | 0 | -9.2 | 5.095 |

**Table 6.1:** Weight distribution estimation

| Configuration | xCog (cm) | Hiatus (cm) | Static Margin (%) | Neutral Point (cm) | $W/S_w$ (kg/$m^2$) |
|---|---|---|---|---|---|
| **Empty Aircraft** | 8.6 | 55 | 33.6 | 16.1 | 3.27 |
| **2 kg of Payload** | 11.3 | 55 | 16.45 | 15 | 6.56 |
| **4 kg of Payload** | 11.6 | 55 | 14.5 | 15 | 10.78 |

**Table 6.2:** Main Characteristics

## 6.2. Aerodynamic derivatives

To analyze the aircraft's behavior under different conditions, the main aerodynamic stability and control derivatives are presented and discussed in Tables 6.3 and 6.4. For this analysis, the team used XFLR5, a panel method-based software capable of evaluating both longitudinal and lateral-directional derivatives.

$C_{M_\alpha}$ represents the rate of change of the pitching moment coefficient with respect

to the angle of attack. For the aircraft to be longitudinally stable, this derivative must be negative, meaning the aircraft generates a restoring moment that opposes increases in angle of attack [4].

Moving on to the lateral-directional derivatives, $C_{N_\beta}$, $C_{N_r}$, and $C_{N_p}$ represent the variation in yawing moment due to sideslip and angular velocities. Similarly, for rolling moment, $C_{l_\beta}$, $C_{l_p}$, and $C_{l_r}$ capture these effects. These parameters are critical for assessing the aircraft's stability, and the sign convention used is outlined in Table 6.3.

| **Configuration** | $\boldsymbol{CM_\alpha}$ | $\boldsymbol{CN_\beta}$ | $\boldsymbol{CN_p}$ | $\boldsymbol{CN_r}$ | $\boldsymbol{Cl_\beta}$ | $\boldsymbol{Cl_p}$ | $\boldsymbol{Cl_r}$ |
|---|---|---|---|---|---|---|---|
| **Desired values** | $< 0$ | $> 0$ | $< 0$ | $< 0$ | $< 0$ | $< 0$ | $> 0$ |
| **Empty Aircraft** | -1.68 | 0.13 | -0.024 | -0.138 | -0.034 | -0.474 | 0.093 |
| **2kg of Payload** | -1.02 | 0.12 | -0.024 | -0.13 | -0.046 | -0.477 | 0.122 |
| **4kg of Payload** | -0.94 | 0.12 | -0.028 | -0.129 | -0.048 | -0.478 | 0.132 |

**Table 6.3:** Main Stability Parameters

| **Configuration** | **Control Surface** | **Efficacy** | **Induced yaw/roll** |
|---|---|---|---|
| **Empty version** | Ailerons | $Cl_{\delta A} = 0.44$ | $CN_{\delta A} = 0.02$ |
| | Elevator | $CM_{\delta E}$ = -1.89 | |
| | Rudder | $Cl_{\delta R} = 0.04$ | $CN_{\delta R}$ = -0.13 |
| **2kg of Payload** | Ailerons | $Cl_{\delta A} = 0.44$ | $CN_{\delta A} = 0.02$ |
| | Elevator | $CM_{\delta E}$ = -1.85 | |
| | Rudder | $Cl_{\delta R} = 0.05$ | $CN_{\delta R}$ = -0.13 |
| **4kg of Payload** | Ailerons | $Cl_{\delta A} = 0.44$ | $CN_{\delta A} = 0.02$ |
| | Elevator | $CM_{\delta E}$ = -1.84 | |
| | Rudder | $Cl_{\delta R} = 0.05$ | $CN_{\delta R}$ = -0.13 |

**Table 6.4:** Main Control Derivatives

The main control derivatives of the aircraft are close to the target values; however, the primary concerns are associated with the ailerons. These control surfaces have been oversized to be used as flaperons during take-off, which results in suboptimal yaw dynamics that are tolerable, as this tradeoff proves rewarding in terms of scoring.

## 6.3. Dynamic analysis

In the analysis of both longitudinal and lateral dynamics, several key parameters are considered. For the longitudinal case, $C_{M_\alpha}$ is negative in both configurations, confirming longitudinal static stability. The eigenvalues associated with the longitudinal and lateral dynamic modes are presented in Table 6.5.

| | Longitudinal Stability | | Lateral Stability | | |
|---|---|---|---|---|---|
| **Configuration** | **Phugoid** | **Short period** | **Roll** | **Dutch roll** | **Spiral divergence** |
| **Empty Aircraft** | $-11.5 \pm 7.5i$ | $0.007 \pm 0.6i$ | $-34.8$ | $-1.5 \pm 6.4i$ | 0.07 |
| **2kg of Payload** | $-8.7 \pm 10.1i$ | $-0.001 \pm 0.5i$ | $-32.6$ | $-1.5 \pm 8.7i$ | 0.06 |
| **4kg of Payload** | $-8.4 \pm 11.4i$ | $-0.002 \pm 0.4i$ | $-29.5$ | $-1.6 \pm 9.9i$ | 0.06 |

**Table 6.5:** Lateral an Longitudinal modes

Both spiral and short period (only on empty configuration) modes are unstable, as indicated by the positive real part of their corresponding eigenvalues. However, those modes develop slowly due to their long characteristic times, allowing the pilot sufficient time to correct the deviation. Figure 6.1 illustrates this phenomenon, which requires corrective action from the pilot.

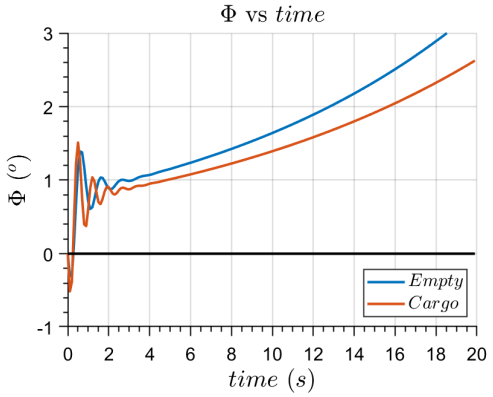


**Figure 6.1:** Roll with side wind gusts

## 6.4. Trim

To achieve a stable, level flight, the pilot must trim the aircraft using the control surfaces. The team analyzed the elevator deflection required to balance the aircraft in longitudinally stable flight, assuming negligible wind drift. Figure 6.2a illustrates the necessary elevator deflection. Conversely, Figure 6.2b shows the pitching moment coefficient without elevator input. The goal of the design is to bring the moment coefficient as close to zero as possible at the equilibrium angle of attack, which is higher in the cargo configurations.

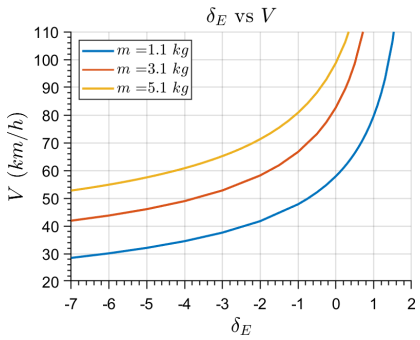


**(a)** Elevator action

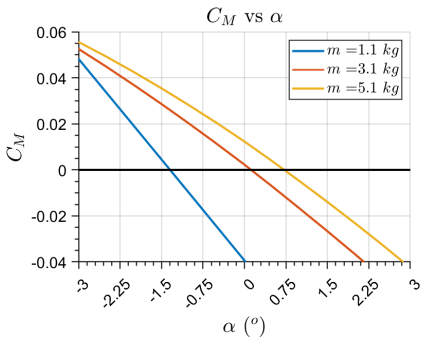


**(b)** Moment coefficient without controls

**Figure 6.2:** Longitudinal moment coefficient

# 7. Aircraft Performance

This section analyzes the aircraft's performance across different configurations, reflecting three operational conditions based on mission requirements. The first scenario corresponds to the aircraft in its Operating Empty Weight (OEW) configuration, without the cargo bay. In the second and third scenarios, the cargo bay is included with payloads of 2 kg and 4 kg, respectively. The key performance data is presented in Figure 7.1 and Table 7.1.

In order to estimate the minimum turning radius, the aerodynamic limitations due to the main lift coefficient and the maximum load factor turn into the two main limitations for the turning radius. The maximum load factor for the aircraft has been estimated to a value of 5, as the experience of the team building such models gives us a reasonable reference for the structural limits.

For the calculation of the take-off velocity, it is assumed to be 1.2 times the stall velocity with flaps down.

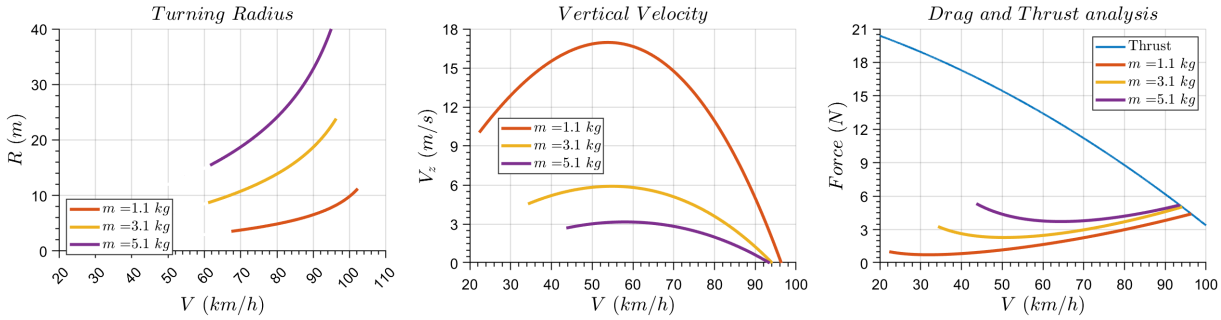


**(a)** Turn radius **(b)** Vertical velocity **(c)** Drag against Thrust

**Figure 7.1:** Aerodynamic performance of the cargo configuration

| Configuration | Take-off distance (m) | $V_{zmax}$ (m/s) | $V_{cruise}$ (km/h) | $V_{TO}$ (km/h) | Minimum turn radius (m) |
|---|---|---|---|---|---|
| **Empty Aircraft** | 5.08 | 16.96 | 96.38 | 25.84 | 3.91 |
| **2kg of Payload** | 18.09 | 5.9 | 94.15 | 39.78 | 9.68 |
| **4kg of Payload** | 36.01 | 3.17 | 93.55 | 50.71 | 17.29 |

**Table 7.1:** Aircraft Performance

The team has concluded that the aircraft is capable of carrying 4 kg of Payload, which corresponds to the maximum payload limit established by the rules.

# 8. Structural Design and Manufacturing

The structure of the aircraft can be divided into four main points of interest: the wing, the fuselage, the payload bay and the empennage.

## 8.1. Wing design

The aircraft features a wood and 3D-printed internal structure reinforced with carbon fiber elements. In 8.1, the final wing design is shown:

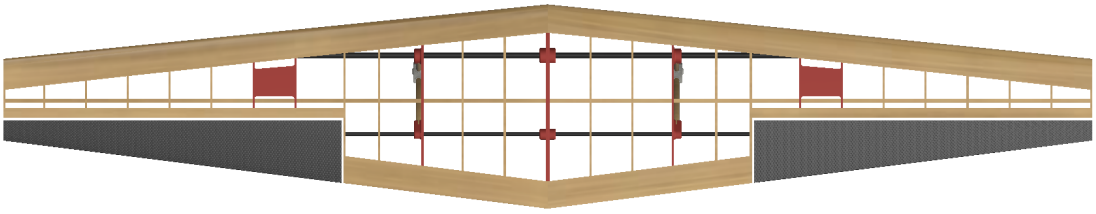

**Figure 8.1:** Final wing structure

Each half wing consists of 14 ribs, 10 of them made of balsa wood and the remaining four out of 3D-printed PLA plastic. The PLA plastic ribs have structural elements integrated into them, such as the landing gear support and the wing to fuselage joint. This design ensures a lightweight yet strong piece. These ribs are highlighted in colour red in Figure 8.1.

Along the span of the wing, five main spars handle the wing loadings. The two main spars are made out of carbon fiber, and three additional balsa wood and plywood spars help distribute the loads. In the next section, further details about how the spars make the wing handle the load will be commented.

The control surfaces of the airplane, the flaperons, have a foam core with a carbon fiber shell. This ensures a lightweight, yet simple and strong structure. Finally, the wing is covered in a thermoplastic wrapping, giving the wing its skin.

## 8.2. Empennage design

The tail empennage structure consists of panels with a foam core, specifically extruded polystyrene (also known as XPS), covered by a low-density carbon fiber sandwich skin. The smooth finish achieved on the skin is the result of a technique that involves placing Mylar sheets over the fibers during the vacuum process, resulting in a much more uniform surface, which helps reduce aerodynamic drag. As for the control

surface hinges, they are reinforced with an aramid strip embedded within the sandwich structure.

Additionally, the empennage is attached to the carbon tube using a 3D-designed and printed part, which is fastened with an M4 screw and secured with structural adhesive to ensure a permanent, failure-resistant bond. The panels also incorporate two rods, one made of 8 mm carbon fiber and another made of 6 mm pine wood, which are inserted and fixed into the 3D-printed part through two dedicated holes, also using structural adhesive. Instead of a wheel, the team has opted for a ski-style design.

**Figure 8.2:** Design of the empennage joint

Finally, this connecting piece includes a light structure onto which the servomotors associated with the empennage control surfaces are mounted and secured with screws.

## 8.3. Payload bay design

The payload bay has a unique design that combines laser-cut elements with fiberglass lamination. The internal structure is made out of plywood ribs, joined together with a squared-section aluminium beam.

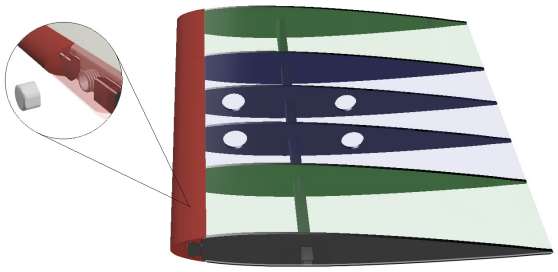

**Figure 8.3:** Design of the payload bay

The ribs divide the bay into three compartments, as seen in Figure 8.3, of (approximately) 2l, 1l and 1l. When the aircraft flies without payload, the bay is removed. For the 2l flight round, the bay is put into position and tightly fixed with screws, and only the center 2l is filled. For the 4l round, all tanks are filled. Each of the compartments is filled from a cap, that lies inside the leading edge of the airfoil, as seen in the detailed view of 8.3. This internal structure is covered in a fiberglass layer, ensuring a watertight seal of the walls.

## 8.4. Wing structural assessment

Numerous tests have been carried out in order to better estimate the wing's strength and overall structural performance, ensuring a safe flight.

In Tables 8.1 and 8.2, the main mechanical properties of the materials are listed:

| **Property** | **PLA** | **PETG** | **Polypropylene** |
|---|---|---|---|
| Density (kg/m$^3$) | 1250 | 1270 | 900 |
| Young's Modulus (GPa) | 3.0–3.5 | 2.1 | 1.5–2.0 |
| Ultimate Tensile Strength (MPa) | 45–65 | 50–70 | 30–40 |
| Compressive Strength (MPa) | 50–70 | 55–75 | 20–30 |
| Poisson's Ratio | 0.36 | 0.38 | 0.42 |

**Table 8.1:** Mechanical properties of PLA, PETG and PP

| **Property** | **Balsa Wood** | **Carbon Fiber** | **Fiberglass** | **XPS** |
|---|---|---|---|---|
| Density (kg/m$^3$) | 160 | 1600 | 1850–2000 | 35 |
| Young's Modulus (GPa) | 3.0 | 230 | 70–85 | 0.03–0.35 |
| Ultimate Tensile Strength (MPa) | 20–30 | 600–1000 | 500–900 | 0.2–0.7 |
| Compressive Strength (MPa) | 10–15 | 500–800 | 250–500 | 0.2–0.6 |
| Poisson's Ratio | 0.3 | 0.2 | 0.22–0.30 | 0.1–0.3 |

**Table 8.2:** Mechanical properties of remaining materials.

### 8.4.1. Flight envelope

The v-n diagram, also known as the flight envelope diagram, is a visual representation of the aircraft's structural and aerodynamic limitations at a certain weight and altitude. On the horizontal axis the speed is displayed (in m/s), and in the vertical axis the load factor is displayed. The region between the stall curves, the load factor limiting lines and the dive speed (maximum speed) is where the plane can safely fly in without causing structural damage to the airframe. [5] For this diagram, the 4l configuration of the airplane will be considered, alongside a maximum cruise altitude of 120m.

To obtain the most accurate diagram possible, a finite element analysis (FEA) was conducted using the ANSYS software suite. A pressure distribution of the wing is obtained in the ANSYS CFD dedicated software Fluent. This data then can be referenced in the FEA. To simplify the analysis, only a half-wing is used, with a fixed constrain in the wing's root, and by symmetry the parameters of the wing are obtained.

The maximum load factor that the wing can handle is approximately 5G, at which point the balsa wood spars and ribs start to be compromised. With data about the wing (CLmax, surface area), the weight of the aircraft and the flight speed, the v-n diagram is plotted.

It is important to note that, in the standard plot of the flight envelope, the diagram is cut at the negative load factor of n = -1. However, to better show the wing's envelope, it has been decided to plot the full diagram until failure, thus it cuts at n = -4G.

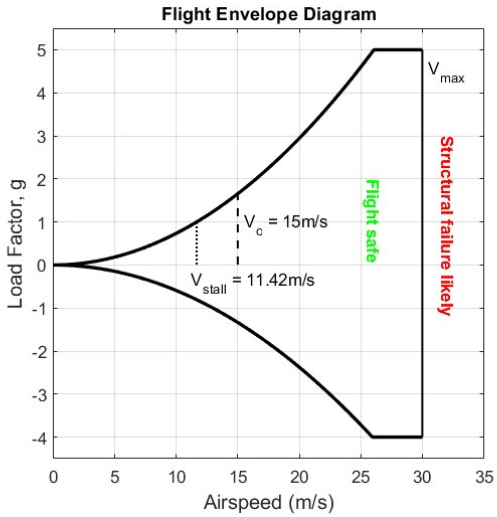


**Figure 8.4:** Flight Envelope Diagram

From this diagram, it can be seen that the prototype should be able to handle its flight profile without compromising the airplane structure. Furthermore, tight turns can also be made up until a wing loading of 5G. To better understand this, the airplane flying at its cruise speed can make a turn of radius 3.91 m without its structure being significantly affected.

### 8.4.2. Stress and bending moment diagrams

To obtain the stress and bending moment diagrams of the wing, the wing will be considered as if it were a beam. The setup consists in the beam, which is fixed in one end and free on the other, and the lift distribution over the wing. The stress and bending moment diagrams, and the lift distribution function are shown in Figure 8.5:

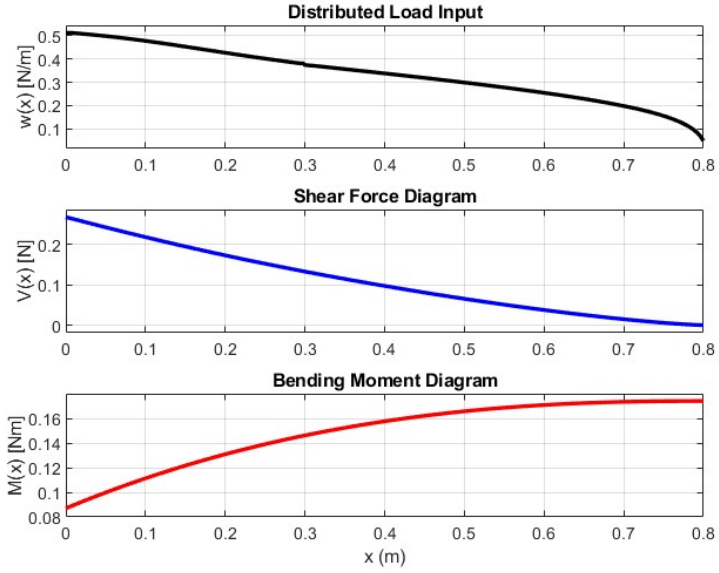


**Figure 8.5:** Stress and bending moment diagrams

### 8.4.3. Wing strength estimation

In addition to previous structural assessments, a standard strength test is to be conducted. The test consists of lifting the fully loaded plane (with bay, 4l) from the tips of the main wing. This gives an idea of how strong the wing is. This test has been performed both in ANSYS software and with the prototype. [6]

For the ANSYS software test, a half wing FEA analysis is conducted, with the root fixed and a upwards force of 25N in the wing tip, simulating the estimated weight (approximately 5kg) of the fully loaded prototype. In Figure 8.6, the result of the total deflection of the wing is shown:

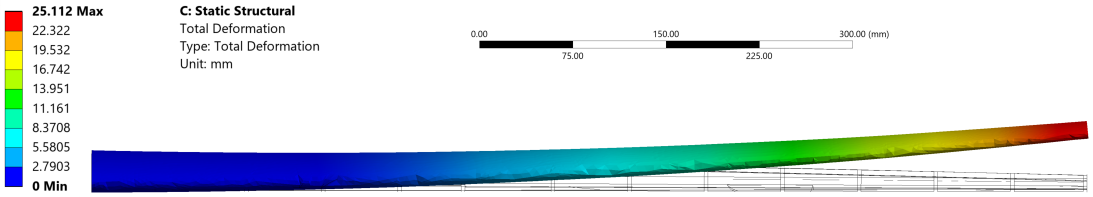


**Figure 8.6:** Total deformation of the wing (ANSYS analysis)

For the real-life test, two 2.5kg weights are placed in the middle of the wing, and two supports are placed near the tip of the wing. In Figure 8.7, the test can be seen:

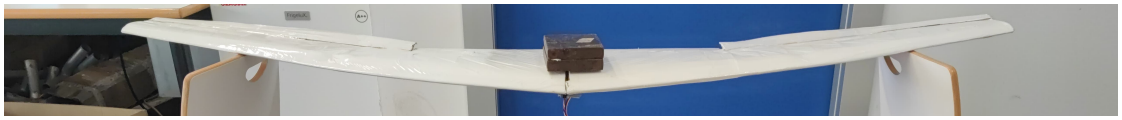

**Figure 8.7:** Test performed on the wing

By comparing both results, it can be assumed that the wing shouldn't suffer major structural failure in flight. Also, the maximum deflection observed in the ANSYS test (25.112mm) is similar to the one observed in the bulit wing, suggesting that the final manufacturing is accurate to the 3D design.

## 8.5. Manufacturing Process

The prototype manufacturing process is divided into several stages, including the construction of the tail, wing, and bay.

### 8.5.1. Wing Manufacturing

The wing is constructed using a robust framework composed of balsa wood and plywood components, reinforced with carbon fiber tubes and 3D-printed ribs made from PLA and PETG. The wing is then covered with Oracover, selected for its minimal weight.

Although the initial flaperon was fabricated using wood and Oracover, technically feasible, it was determined that a sandwich structure of extruded polystyrene (XPS) and carbon fiber yielded a significantly lighter component, more suitable for the low-density, small surface area.
For assembly, once the wooden elements are laser-cut and the 3D-printed parts are ready, a full-scale plan is employed to guide positioning. The structural pieces are bonded using wood glue due to its strength and low weight.

Once fully dry, the servos are installed, wiring is completed, and nylon hinges are attached to link the control surfaces to the main wing. The covering process then begins, with Oracover applied in two sections per wing half, adapting to the curvature around the flaperon. A single piece of covering is used for the flaperon section, with another covering the remaining span, optimizing the finish quality.

**Figure 8.8:** Wing assembly

To finalize the flaperon, the XPS core is CNC machined, and laminated. Low-density carbon fiber sheets are trimmed to size and used along with epoxy resin to bond them to the core. The laminated component is then sealed in a vacuum bag until fully cured.

### 8.5.2. Empennage Manufacturing

This process closely mirrors that of the flaperons, with some modifications. In addition to carbon fiber, Mylar sheets are introduced to achieve a smoother aerodynamic finish and ensure laminar airflow. After cutting the core, fiber impregnation is performed.

Reinforcement rods are inserted into the XPS, and aramid fibers are used to strengthen the hinge zones destined for control surfaces. Unidirectional carbon fiber is also applied along the leading edge, chosen for its moldability, structural integrity, and superior finish. Following fiber application, Mylar sheets are affixed to both upper and lower panel surfaces before vacuum curing.

**Figure 8.9:** Panel finish

**Figure 8.10:** Final Empennage

### 8.5.3. Bay Manufacturing

Although this section also employs lamination techniques, the method differs. A 3D-printed positive mold is used as a base. After multiple layers of mold release agent are applied to prevent adhesion, the epoxi-impregnated fiber is layed up.

Three layers of fiberglass are applied over the mold, providing enhanced strength and water resistance. These are saturated with epoxy resin and cured in a vacuum bag. Post-curing, the component is removed and the mold is detached. Plywood ribs are then positioned using set squares and bonded with structural adhesive to define the internal compartments. Said ribs are sealed with epoxi to waterproof them.

Cap thread fittings, also 3D-printed, are installed by drilling appropriately sized holes into the bay's top face. These threads are glued in with structural adhesive. The caps themselves, made of polypropylene, are screw-mounted, providing watertight yet accessible filling and drainage. After this, the whole bay is sprayed with spray sealant, to seal any remaining pores. Finally, the leading edge is 3D printed and mounted to the bay's front face caps via integrated rails.

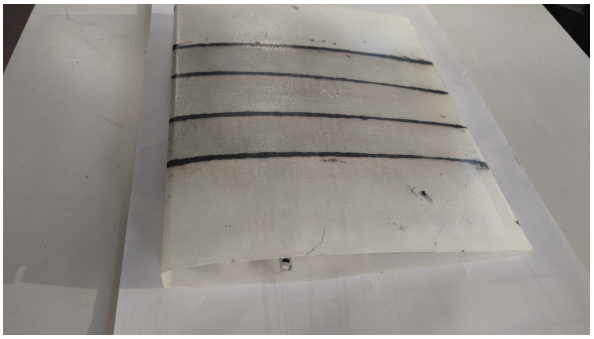

**Figure 8.11:** Fiberglass structure manufacturing of the bay

# 9. Outlook

In this final section, the current state of the team, from the submittal of the report, to the dates of the competition, is analized.

As disclosed, propeller testing has been done, both on a testbed and in flight, allowing the plane to get the most out of the motor.

A technology demonstration aircraft has also been built and flown. Through five completed flight tests, the team has achieved a strong proof of concept. Thanks to this, problems have been fixed and ideas tested:

The wing structure is more than robust enough to carry the load. By manufacturing the wing early, the structural design was revisited in order to obtain a more polished and lighter design.

The same can be said for the tail. Components have been redesigned to make them lighter, as mentioned, in order to obtain a higher competition score.

The manufacturing method of the cargo bay has also been changed. Initially, a fully 3D printed cargo bay out of polypropilene was built. This caused problems as the water would escape out of the z-hops in between layers, and as nothing sticks to this material due to its low surface tension, it cannot be properly sealed. The revisited design out of composite proves to be a more trustworthy and robust design, improving also the stability of the aircraft.

In the upcoming weeks before the competition, the final aircraft will be built and flown. This will allow the pilot to become more comfortable with the aircraft in its various configurations. The aircraft assembly process will also be practiced, in order to do this faster during the competition.

**Figure 9.1:** XTRA26 "Sísí" maiden flight

# Bibliography

[1] Zbigniew Czyż, Paweł Karpiński, Krzysztof Skiba, and Mirosław Wendeker. Wind tunnel performance tests of the propellers with different pitch for the electric propulsion system. *IEEE International Workshop on Metrology for AeroSpace)*, 2021.

[2] Daniel P. Raymer. *Aircraft Design: A Conceptual Approach.* American Institute of Aeronautics and Astronautics, Reston, Virginia, 5th edition, 2012.

[3] Jose Carlos Morcillo Morcillo. Análisis, diseño y fabricación de un aeromodelo orientado a la maximización de la carga de pago para la competición air cargo challenge. Technical report, Universitat Politècnica de València, November 2021.

[4] Marcello R. Napolitano. *Aircraft Dynamics: From Modeling to Simulation.* Wiley, Hoboken, New Jersey, 2nd edition, 2012.

[5] IVAO documentation library. *Flight envelope.*

[6] Ansys, https://innovationspace.ansys.com. *Ansys Innovation Space.*